applied sciences

MDPI

Article

High Frequency Bipolar Electroporator with Double-Crowbar Circuit for Load-Independent Forming of Nanosecond Pulses

Vitalij Novickij [1,*], Gediminas Staigvila [1], Arūnas Murauskas [1], Nina Rembialkowska [2], Julita Kulbacka [2] and Jurij Novickij [1]

[1] Faculty of Electronics, Vilnius Gediminas Technical University (VilniusTECH), 03227 Vilnius, Lithuania; gediminas.staigvila@vilniustech.lt (G.S.); arunas.murauskas@vilniustech.lt (A.M.); jurij.novickij@vilniustech.lt (J.N.)

[2] Department of Molecular and Cellular Biology, Faculty of Pharmacy, Wroclaw Medical University, 50-556 Wrocław, Poland; nina.rembialkowska@umed.wroc.pl (N.R.); julita.kulbacka@umed.wroc.pl (J.K.)

* Correspondence: vitalij.novickij@vilniustech.lt

Abstract: In this work, a novel electroporation system (electroporator) is presented, which is capable of forming high frequency pulses in a broad range of parameters (65 ns–100 µs). The electroporator supports voltages up to 3 kV and currents up to 40 A and is based on H-bridge circuit topology. A synchronized double crowbar driving sequence is introduced to generate short nanosecond range pulses independently of the electroporator load. The resultant circuit generates pulses with repetition frequencies up to 5 MHz and supports unipolar, bipolar, and asymmetrical pulse sequences with arbitrary waveforms. The shortest pulse duration step is hardware limited to 33 ns. The electroporator was experimentally tested on the H69AR human lung cancer cell line using 20 kV/cm bipolar and unipolar 100 ns–1 µs pulses. Based on a YO-PRO-1 permeabilization assay, it was determined that the electroporator is suitable for applied research on electroporation. The system offers high flexibility in experimental design to trigger various electroporation-based phenomena.

Keywords: electroporation; generator; square wave; crowbar; MHz pulses

check for updates

Citation: Novickij, V.; Staigvila, G.; Murauskas, A.; Rembialkowska, N.; Kulbacka, J.; Novickij, J. High Frequency Bipolar Electroporator with Double-Crowbar Circuit for Load-Independent Forming of Nanosecond Pulses. *Appl. Sci.* **2022**, *12*, 1370. https://doi.org/10.3390/app12031370

Academic Editor: David García Fresnadillo

Received: 5 January 2022
Accepted: 26 January 2022
Published: 27 January 2022

1. Introduction

Electroporation is a transient or permanent increase in biological cell membrane permeability when subjected to high intensity electric field pulses [1]. The treatment outcome depends on the pulse parameters, including waveform, duration, amplitude, frequency, etc. [2,3]. As a result, pulsed power electronics became an inseparable part of electroporation or techniques associated with this method. Therefore, the development of pulsed power systems for electroporation, known as electroporators, is constant [4–10].

With the development of semiconductor technology, the area of electroporation applications is also transitioning towards a shorter pulse range (i.e., use of nanosecond pulses) [11–14]. The short but high intensity pulses can target intracellular structures without porating the cell itself [15,16]. Additionally, with the use of nanosecond protocols, modulation of cell death is possible, which is useful to minimize inflammation of the tissue [17]. Recent developments show the high potential of the high frequency irreversible electroporation (H-FIRE) methodology when sequences of high frequency pulses are used to permeabilize the cells [18–20]. At the same time, the 100 kHz–10 MHz pulse repetition range is poorly covered due to a lack of technological infrastructure.

To address the problem, in the past 2–3 years, a variety of novel high frequency electroporation systems were proposed. In 2019, Redondo et al. presented solid-state unipolar positive Marx generators positioned back to back to generate high frequency bipolar pulses [21]. The system is capable of forming up to 5 kV bipolar pulses, with 500 ns–10 µs pulse widths and 200 ns–10 µs relaxation times between positive and negative pulses. In 2021, Pirc et al. showed a prototype of an asymmetric bipolar pulse generator [22].

The developed device is able to generate up to 4 kV pulses with a minimal 200 ns duration and 2 MHz pulse repetition frequency. In 2018, Ryan et al. presented a prototype with multiple stacks of MOSFETs in parallel to create multiphase outputs with pulses as short as 80 ns [23]. Recently, Kandratsyeu et al. published a 6.5 kV four-channel generator for 100 ns–100 µs pulses for use in biomedical applications [24]. In all cases, silicon-carbide (SiC) MOSFETs were used, which became a popular technology for the generation of high frequency high power bursts [25].

One of the problems, which is common for sub-microsecond pulse forming systems, is the impedance matching to prevent any reflections [26]. In the electroporation context, depending on the cell buffer, tissue heterogeneity, type, and structure of electrodes, the impedance of the load may vary from tens of Ω [27] to several kΩ [28]. Therefore, quite frequently, the electroporator is shunted with sub-100 Ω resistance. This is a sub-optimal solution since it draws almost double the power from the generator and also does not solve the impedance matching problem completely. The impedance will still vary since the load is connected in parallel with the shunting resistance. To solve the problem, we have previously proposed a unipolar electroporation system featuring a controlled crowbar circuit [4], which cuts the pulse fall-time and, thus, ensures constant rise and fall times independently from the load. A similar concept was recently used by Stankevič et al. [5]. In the context of electroporation, ensuring constant rise and fall times is crucial due to the dependence of the biological effects on the polarization of the cellular membrane [29].

In this work, we wanted to combine the various recent electroporator concepts into one machine and produce a novel multiphasic electroporation system. The new system must support pulse repetition frequencies higher 1 MHz, feature a double-crowbar circuit to diminish the impedance matching problem, and be capable of generating pulses shorter than 200 ns. All these parameters combined in a device could be a worthy improvement for state-of-the-art electroporation studies and become a competitive addition to the in-house-made prototype family, which is available in the literature.

2. Materials and Methods

2.1. Pulse Forming Circuit

The pulse forming circuit is based on a standard H-bridge topology, operated in a synchronized double-crowbar mode. The simplified scheme is shown in Figure 1.

It can be seen that the circuit has 8 MOSFET switches T_1–T_8 (C2M0080120D, Cree Inc., Durham, NC, USA), with two switches in each wing. For pulse forming, 4 switches are driven in synchronization (i.e., T_1–T_4 or T_5–T_8), which enables a bipolar pulse shape. However, the dynamic characteristics of a MOSFET are load-dependent, therefore, a synchronized double-crowbar driving circuit is introduced. It implies that after each pulse, an additional wing is opened to shunt the circuit (e.g., when T_1–T_4 are going to be closed to end the pulse, the T_7, T_8 are opened at the same time). Therefore, a second route for the current is formed, which is limited only by R_{LIM} = 10 Ω, thus a minimum fall time of the pulse is ensured. The capability to form MHz range and sub-microsecond pulses is the most important factor to ensure the novelty of the electroporator, therefore, it is counter-productive to use lots of series switches due to the respective increases in the rise and fall times. However, the use of series switches is required to increase the handling voltage. As a result, the circuit had to be designed to feature minimum parasitic inductance and still have a reserve in terms of breakdown voltage to account for reverse voltage during maximum loads (~40 A). The breakdown voltage of a single switch is 1.2 kV, thus when switches are used in an array of 4, the total breakdown voltage is 4.8 kV. However, during pulse forming (a stage is opened), for the whole duration of the pulse, the charging voltage is distributed only between two switches (either the pair of T_7, T_8 or T_3,

This implies that when the device is charged to 3 kV, the voltage is already exceeding the datasheet ratings. Nevertheless, it was empirically determined that such an overvoltage (3 kV versus 2.4 kV) is still within the handling range of the used SiC MOSFETs, but the pulses must be limited to 1 ms. Additionally, when the crowbar is opened, up to

300 A currents are induced. However, we have limited the operation of the crowbar to 65–100 ns, which again is not sufficient to thermally destroy the pn junction. All the solutions combined to make a trade-off between the number of switches, the handling voltage, and the dynamic characteristics of the circuit. T_4).

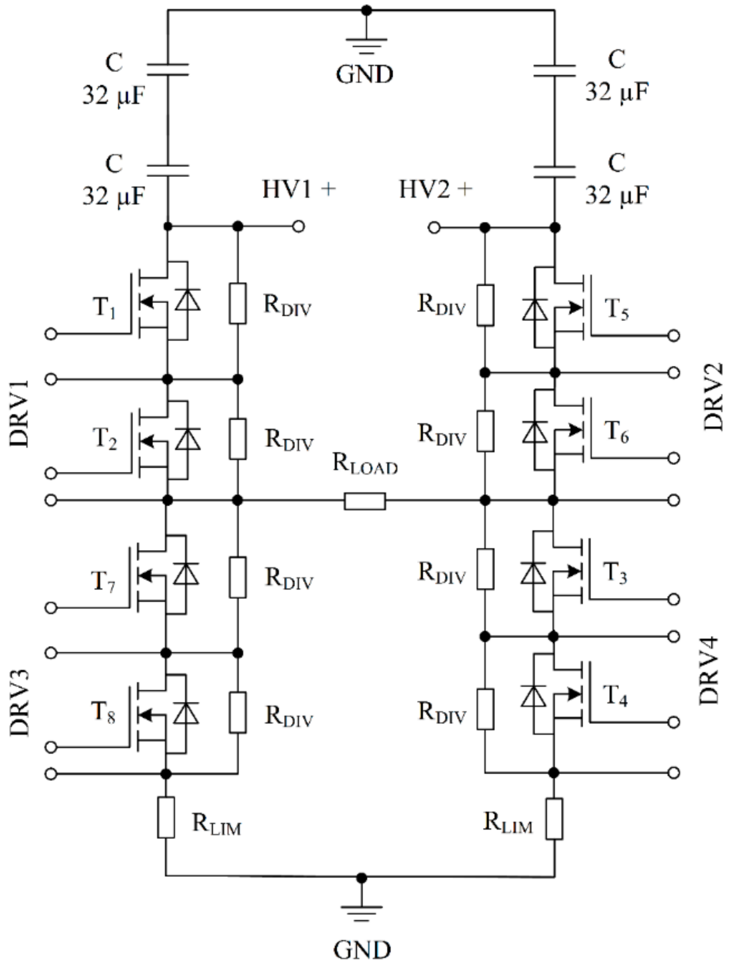

Figure 1. The pulse forming circuit of the electroporator, which is based on H-bridge circuit topology.

As high voltage sources, two UM4P30 (Spellman High Voltage Electronics Corp., Hauppauge, NY, USA) voltage supplies were used. The R_{DIV} = 1 MΩ were used as bleeder resistors to equally distribute the DC voltage. The capacitor array included two capacitors in each stage (32 µF, KEMET MKP C4AQ, Fort Lauderdale, FL, USA).

2.2. Driving Circuit

A fast galvanically decoupled driving circuit had to be introduced to enable MHz switching with sub-100 ns pulses. Therefore, we introduced a 3-stage, 8-channel driver including a microcontroller, the main driver (DRV0), and the respective drivers for MOSFETs (DRV1-4). The simplified block scheme is shown in Figure 2.

The microcontroller was a 32 MHz XMEGA128A3U (Atmel, San Jose, CA, USA) operating at 3.3 V, which was driving the main 4-channel ADUM140D0BRWZ driver (Analog Devices Inc., Norwood, MA, USA). This stage was introduced to make the driving signal 5 V and galvanically decoupled, ensuring better resistance to ground bouncing and electromagnetic noise. The DRV1–DRV4 were the ADUM4223ARWZ (Analog Devices Inc., Norwood, MA, USA) operated at 15 V and limited by a gate resistance of 4.7 Ω. Connecting the microcontroller directly to DRV1–DRV4 was unsuccessful due to high electromagnetic noise.

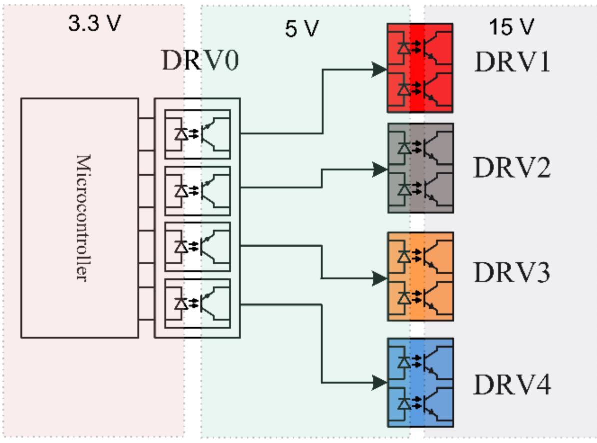

Figure 2. The block diagram of the driving circuit.

2.3. The Prototype and Testing

The PCB board (double-sided FR-4) was fabricated by JLCPCB (Krefeld, Germany), and the final prototype assembled and tested at Vilnius Gediminas Technical University (VilniusTECH). The photograph of the electroporator prototype is shown in Figure 3.

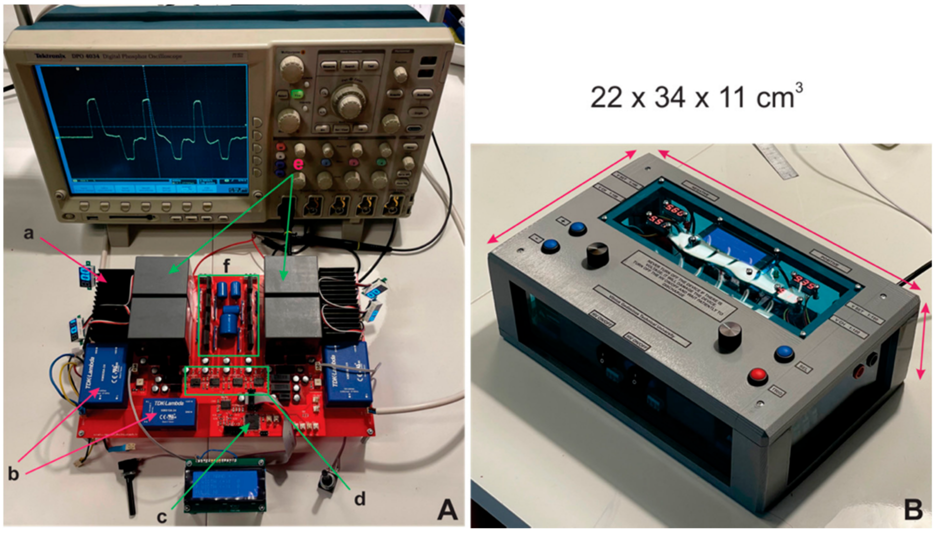

Figure 3. The photograph of the (**A**) electroporator prototype, where a—HV source, b—LV sources with galvanic decoupling, c—microcontroller, d—array of drivers DRV1–4, e—power capacitors, and f—the high-power circuit; (**B**) the final device.

It can be seen that the prototype features a compact design (22 $\times$ 34 $\times$ 11 cm^3). The user interface involves a 4 $\times$ 16 LCD display showing basic pulsing parameters, two potentiometers (control of charging voltage), and 4 buttons (Figure 3B).

All the measured pulses were acquired using a DPO4034 oscilloscope (Tektronix, Beaverton, OR, USA) and P4250 probe (Cleqee, Shenzhen, China) and further post-processed in OriginPro 8.5 software (OriginLab, Northampton, MA, USA).

2.4. Electroporation

The studies were performed in vitro on a human lung cancer cell line (H69AR). The cells were maintained in RPMI (Sigma-Aldrich, Poznan, Poland) supplemented with 5% fetal bovine serum (FBS, Lonza BioWhittaker, Visp, Switzerland), 1% penicillin/streptomycin (Sigma-Aldrich, Poznan, Poland), 0.5% sodium pyruvate (Sigma-Aldrich), and 50 µmol/L 2-mercaptoethanol (Sigma-Aldrich, Poznan, Poland). Cell cultures were cultivated as a monolayer in 25 and 75 cm^2 plastic flasks (Nunc, Roskilde, Denmark), maintained in a humidified atmosphere at 37 °C and 5% CO_2, and detached for the experiments by trypsinization (trypsin 0.025% and EDTA 0.02% solution, Sigma-Aldrich, Poznan, Poland). Cells were passed every 2–3 days and a day before the experiment.

For electroporation, cells were trypsinized and centrifuged (5 min, 1000 rpm, MPW-341 centrifuge with stable rotor, MPW Med. Instruments, Warsaw, Poland). Then, cells were counted and for each sample 5×10^5 of cells were resuspended in HEPES buffer (10 mM, Sigma) containing 250 mM sucrose (POCH, Gliwice, Poland) and 1 mM $MgCl_2$ in Milli-Q water.

Flow cytometry analysis using YO-PRO-1 was performed to evaluate electroporation. Before the pulsing, YO-PRO™-1 iodide (YP-1, λexc491/λem509, Thermo Scientific, Warsaw, Poland) was added to the cell suspension. Final concentration of YP-1 was 1 μM. Flow cytometric analysis was performed using a CyFlow CUBE-6 flow cytometer (Sysmex, Warsaw, Poland). The samples were excited using the 488 nm line of the blue laser and the fluorescence of YP-1 was measured with an FL-1 detector. Data were analyzed using CyView software (Sysmex, Warsaw, Poland).

For electroporation itself, a single unipolar pulse of 20 kV/cm × 200 ns–1 μs was used. Alternatively, the same energy was delivered via bipolar pulse for comparison (e.g., the effects of a 200 ns unipolar pulse were compared to the effects of a 100 ns + 100 ns bipolar pulse). One-way analysis of variance (ANOVA; $p < 0.05$) was used to compare the treatments. A Tukey HSD multiple comparison test for evaluating the difference was used when ANOVA indicated a statistically significant result ($p < 0.05$ was considered statistically significant). All experiments were performed in at least three repetitions, and the treatment efficiency was expressed as mean ± standard deviation.

3. Results

3.1. The Electroporator

In order to describe the operation principle in detail, the DRV0 signals were measured and compared with the resulting waveform on the load (R_{LOAD} = 1 kΩ). The waveforms are shown in Figure 4.

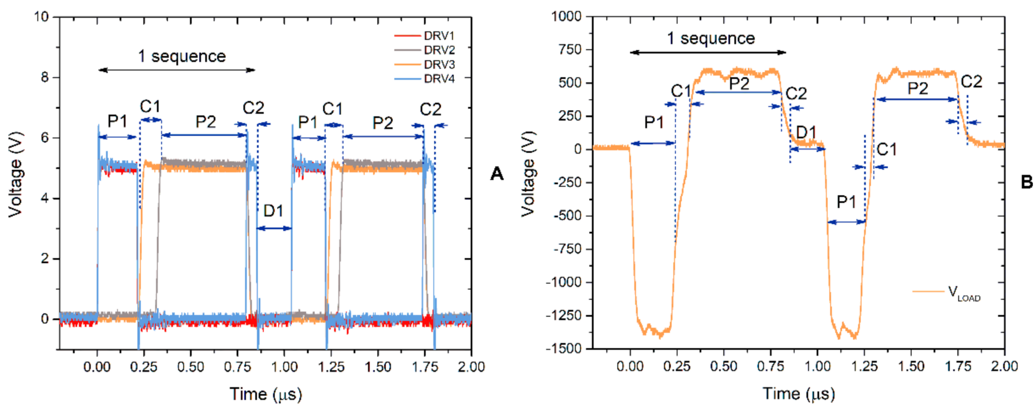

Figure 4. The output waveforms of a 4-channel driver (**A**) and the output pulse on the load (**B**), where P1 and P2 are 200 and 500 ns pulses, respectively; C1 and C2 are the crowbar pulses (sub-100 ns) and D1 is the preprogrammed delay between sequences, which is in this case equal to 190 ns; R_{LOAD} = 1 kΩ.

As can be seen in Figure 4A, firstly, the DRV1 and DRV4 are triggered to form a 200 ns pulse by opening the respective switches (T_1–T_4, refer to Figure 1). Then, a crowbar (C1) is used to rapidly cut the fall time (DRV3 is triggered, which opens T_7 and T_8), followed by a 500 ns pulse of reverse polarity (DRV2 and DRV3 are active to control T_7 and T_8). Similarly, in order to cut the fall time, the second crowbar is used (C2) and, thus, DRV4 is triggered (T_3 and T_4 are open). The effects of such a driving sequence can be observed in Figure 4B. It allows rapid switching of kV range pulses even in kΩ loads. A programmable delay D1 can be introduced between repetitive sequences.

The importance of the crowbar circuit can be highlighted when the prototype is tested with various loads. The effects of the crowbar circuits and pulse waveform dependence on the R_{LOAD} are presented in Figure 5.

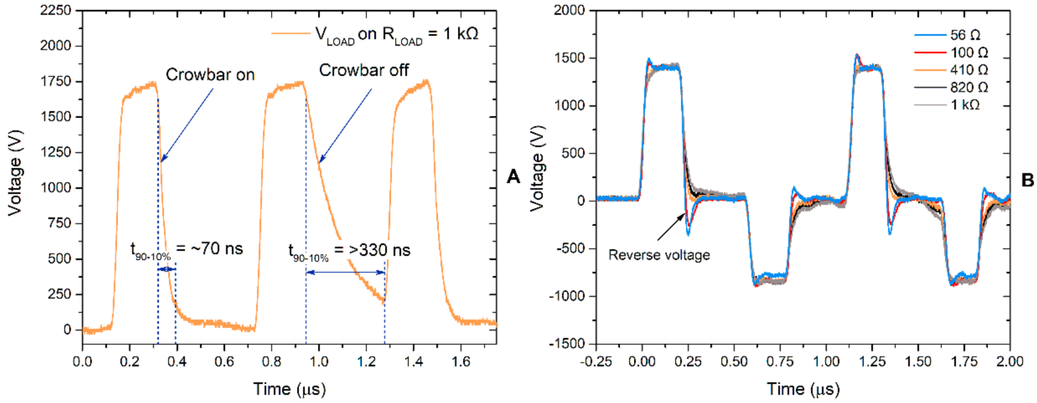

Figure 5. The effects of the crowbar circuit on the pulse waveform (**A**) and the dependence of the output pulse waveform on the load (**B**).

It can be seen in Figure 5A that the crowbar circuit enables the pulse fall time to be in the range of 70 ns. If the crowbar is not involved, the fall time increases dramatically, which is highly undesirable. Further, the generator was tested with various loads to imitate various electroporation conditions. The respective waveforms are shown in Figure 5B.

It can be seen that independently from the load, the pulse features the same waveform with almost identical dynamic parameters. In the case of high power pulses (R_{LOAD} = 56 and 100 Ω), the distributed parasitic inductance of the circuit starts to play a role, therefore, a short reverse voltage spike can be observed. Considering the short duration of the transient process, we believe that compensating the spike with additional snubber circuits is not necessary. However, it can be implemented if required. As was mentioned above, the implementation of snubber circuits will worsen the dynamic characteristics of the generator.

The shortest possible pulses with the highest possible repetitive frequencies were further investigated. The waveforms are presented in Figure 6.

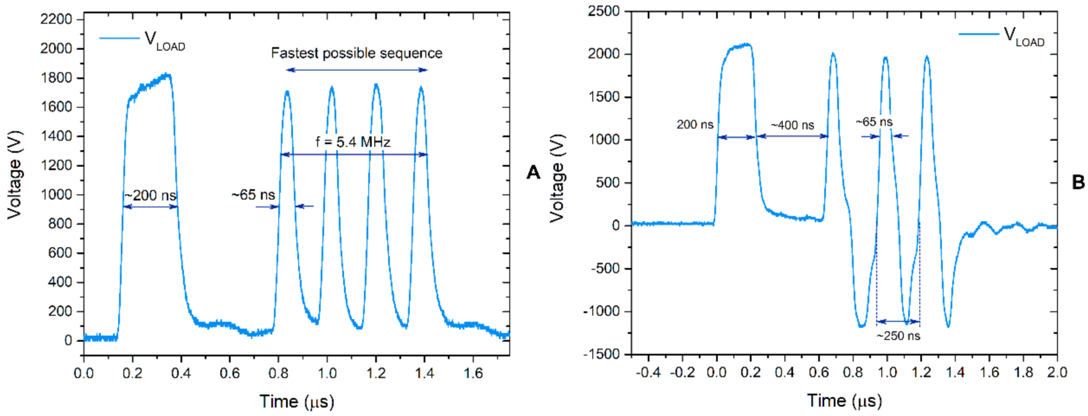

Figure 6. Exemplary high frequency unipolar (**A**) and bipolar (**B**) sequences featuring shortest possible pulses, R_{LOAD} = 1 kΩ.

The first 200 ns pulse was generated for comparison purposes and scaling of the following unipolar and bipolar sequences. In Figure 6A, it can be seen that the fastest possible sequence exceeds 5 MHz repetition frequency with the shortest possible pulse in the range of 65 ns. It is a significant improvement compared to available electroporators. The bipolar sequence (Figure 6B) can also feature a 65 ns waveform with the shortest period of the pulses in the range of 250 ns. A 33 ns step can be introduced to increase the pulse duration, which is a limitation of the microcontroller, which operates at a 32 MHz frequency.

Finally, the capability to form arbitrary waveform sequences was confirmed, and an exemplary waveform is shown in Figure 7.

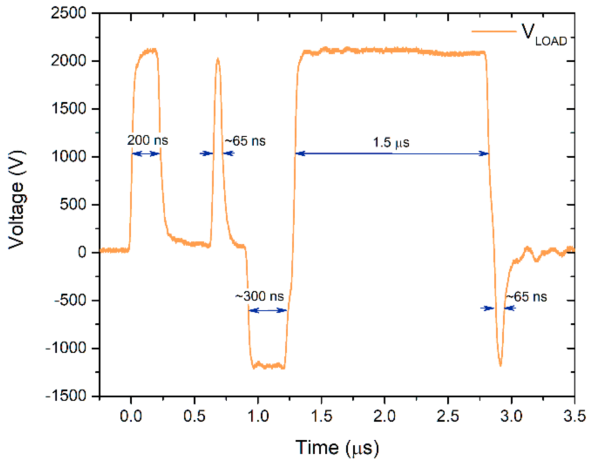

Figure 7. An exemplary arbitrary pulse waveform that can be generated using the proposed electroporator, R_{LOAD} = 1 kΩ.

It can be seen that the pulse shape and polarity, including the delays between separate pulses, can be easily pre-programmed, which offers high flexibility in parametric protocol design. The pulses can be symmetric and asymmetric both in terms of amplitude and duration.

3.2. Electroporation of Cancer Cells

The cells were electroporated using unipolar and bipolar pulses. The results are summarized in Figure 8. It can be seen that in the case of unipolar pulses, the cells are highly permeabilized at 20 kV/cm × 400 ns. However, this is not the case for bipolar pulses. High electroporation efficiency (permeabilized >90% of the cells) is reached only when a 500 + 500 ns pulse is generated, indicating the effects of polarization phenomena during supra-electroporation. For example, the number of permeabilized cells triggered by a 400 ns unipolar pulse when compared to a bipolar 200 ns + 200 ns pair was several fold higher (93% vs. 33%, $p < 0.05$), while the input energy was the same. Capability for precise delivery of pulses of various shapes with high flexibility opens future opportunities for the study of electroporation biophysics, including polarization phenomena.

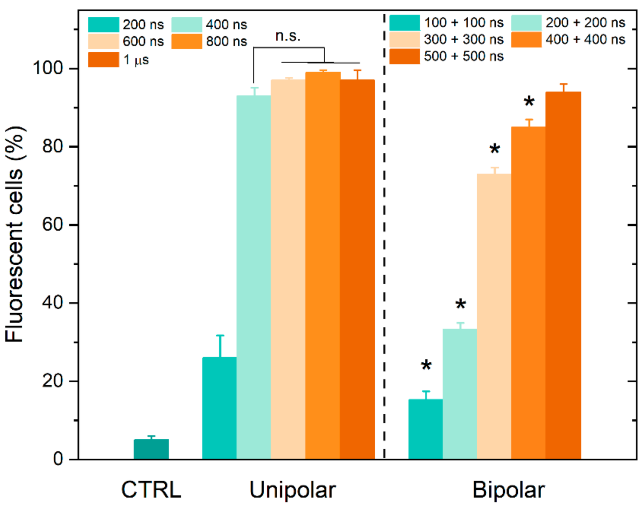

Figure 8. Cell permeabilization triggered by single unipolar and bipolar pulses of 20 kV/cm, where the asterisk (*) corresponds to statistically significant ($p < 0.05$) differences between unipolar and bipolar pulses of identical energy; n.s.—statistically non-significant ($p > 0.05$).

It was successfully confirmed that the developed electroporator is suitable for electroporation research and study of the effects of both unipolar and bipolar pulses.

4. Discussion

In this work, a novel electroporator has been presented, which is based on H-bridge circuit topology and the double-crowbar driving technique. Such an approach enabled the operation of the SiC MOSFETs beyond their datasheet ratings with close to minimal rise and fall times. The summary of the parameters is presented in Table 1.

Table 1. The parameters of the developed electroporator.

Parameter	Value
Voltage	Up to 3 kV
Current	Up to 40 A
Pulse duration	65 ns–100 µs
Duration step	33 ns
Repetition frequency	Up to 5.4 MHz
Pulse shape	Unipolar; bipolar; arbitrary

It should be noted that we have used the latest solutions available, which were provided either by our or other groups, and combined them in one generator. The proposed driving technique allowed us to extend the range of parametrical flexibility. Additionally, the three-stage driving circuit can support a lot more MOSFET drivers, thus the number of MOSFETs in each wing can be at least doubled if higher voltages are required. The number of microcontroller pins will still be four to drive them all. However, it is important to account for the thermal effects in the pn junction of MOSFETs involved in the crowbar wings of the H-bridge topology. In the presented prototype, the current can reach up to 300 A, thus if a higher voltage is used, it is likely that a more powerful MOSFET should be used (e.g., Cree, C2M0045170D). Another advantage of the proposed driving method is the zero relaxation times between opposite phase pulses. This can play a significant role in studying the cancellation effects happening during ultrashort pulses [30].

The limitations of the generator can also be highlighted. Firstly, we limited the generator to 3 kV and 40 A, sufficient for all reversible electroporation applications. However, if irreversible nanosecond electroporation is required, we believe that the number of MOSFETs in a stage should be doubled, which will increase both the voltage and current handling. In such a scenario, we would aim for a 6 kV/80 A device using the same circuit and driving topology we proposed in this paper since it offers good scalability. Additionally, our device is limited by the minimum duration step of 33 ns, which is due to the 32 MHz microcontroller. If better precision is required, either a computer-controlled or/and FPGA interface should be introduced, or/and solutions using auxiliary four-channel low power generators can be implemented too. Nevertheless, the dynamic characteristics of the generator will still be limited by the SiC MOSFET technology as in all other available devices in the literature.

The potential applications and parametrical flexibility of the proposed electroporator can be highlighted as the main factors affecting the novelty and actuality. The short nanosecond pulses enable better control of the energy of the burst due to a significantly higher number of pulses in a sequence and shorter rise and fall times. Compared to the standard microsecond procedures, nanosecond sequences also involve several-fold higher PEF amplitudes, which is beneficial in terms of a more uniform tumor exposure [31]. Additionally, the capabilities to trigger additional cellular mechanisms in the nanosecond pulse range are frequently reported in the literature [32–34]. At the same time, bipolar pulses result in a higher frequency component compared to the unipolar ones, thus the heterogeneity of tumors can be better compensated [35]. Asymmetrical nanosecond pulses can be potentially exploited in the cancellation phenomena [30], providing a base for new and selective electrochemotherapy protocols. Lastly, we speculate that the high frequency nanosecond protocols, which can be derived using the proposed machine, can help to significantly reduce the muscle contractions during the treatment, similar to the H-FIRE procedure [20,36].

To conclude, the developed electroporator is a novel device in the context of electroporation, which enables research of H-FIRE, cancellation phenomena, nano-electrochemotherapy, and beyond. We believe that the 5 MHz pulse compression is a particularly promising application due to recently reported new polarization phenomena in the 1 MHz repetition frequency range [29,37,38]. We have tested it in basic electroporation experiments, which have proven that it is suitable for parametric studies and electroporation research and thus is a good addition to the currently available family of electroporators.

Author Contributions: Conceptualization, V.N. and J.K.; methodology, V.N.; software, V.N.; validation, A.M., G.S. and N.R.; investigation, A.M. and J.N.; resources, V.N.; writing—original draft preparation, V.N.; writing—review and editing, V.N., J.N. and J.K.; supervision, V.N. and J.K.; project administration, V.N. and J.K.; funding acquisition, V.N. and J.K. All authors have read and agreed to the published version of the manuscript.

Funding: This research was funded within the DAINA2 Research framework by the Research Council of Lithuania, grant number S-LL-21-4 (PI: V. Novickij) and by the National Science Centre (Poland) grant DAINA 2 no. 2020/38/L/NZ7/00342; (PI: J. Kulbacka).

Institutional Review Board Statement: Not applicable.

Informed Consent Statement: Not applicable.

Data Availability Statement: Data are available from the corresponding author V.N. on request.

Conflicts of Interest: The authors declare no conflict of interest.

References

1. Kotnik, T.; Kramar, P.; Pucihar, G.; Miklavčič, D.; Tarek, M. Cell membrane electroporation—Part 1: The phenomenon. *IEEE Electr. Insul. Mag.* **2012**, *28*, 14–23. [CrossRef]
2. Pucihar, G.; Krmelj, J.; Reberšek, M.; Napotnik, T.B.; Miklavčič, D. Equivalent pulse parameters for electroporation. *IEEE Trans. Biomed. Eng.* **2011**, *58*, 3279–3288. [CrossRef] [PubMed]
3. Zhao, D.; Wu, M.; Huang, D.; Liang, Z.; Wei, Z.; Li, Z. Parametric optimization of electric field strength for cancer electrochemotherapy on a chip-based model. *Theranostics* **2018**, *8*, 358. [CrossRef] [PubMed]
4. Novickij, V.; Grainys, A.; Butkus, P.; Tolvaišienė, S.; Švedienė, J.; Paškevičius, A.; Novickij, J. High-frequency submicrosecond electroporator. *Biotechnol. Biotechnol. Equip.* **2016**, *30*, 607–613. [CrossRef]
5. Stankevic, V.; Simonis, P.; Zurauskiene, N.; Stirke, A.; Dervinis, A.; Bleizgys, V.; Kersulis, S.; Balevicius, S. Compact Square-Wave Pulse Electroporator with Controlled Electroporation Efficiency and Cell Viability. *Symmetry* **2020**, *12*, 412. [CrossRef]
6. Puc, M.; Flisar, K.; Reberšek, S.; Miklavčič, D. Electroporator for in vitro cell permeabilization. *Radiol. Oncol.* **2001**, *25*, 3.
7. Byagathvalli, G.; Sinha, S.; Zhang, Y.; Styczynski, M.P.; Standeven, J.; Bhamla, M.S. ElectroPen: An ultra-low-cost, electricity-free, portable electroporator. *PLoS Biol.* **2020**, *18*, e3000589. [CrossRef]
8. Pirc, E.; Miklavcic, D.; Rebersek, M. Nanosecond Pulse Electroporator with Silicon Carbide MOSFETs, Development and Evaluation. *IEEE Trans. Biomed. Eng.* **2019**, *66*, 3526–3533. [CrossRef]
9. Imai, F.; De Novaes, Y.R. Design and Assembly of a Bipolar Marx Generator Based on Full-Bridge Topology Applied to Electroporation. In Proceedings of the 2019 IEEE 15th Brazilian Power Electronics Conference and 5th IEEE Southern Power Electronics Conference, Santos, Brazil, 1–4 December 2019.
10. Levkov, K.; Linzon, Y.; Mercadal, B.; Ivorra, A.; González, C.A.; Golberg, A. High-voltage pulsed electric field laboratory device with asymmetric voltage multiplier for marine macroalgae electroporation. *Innov. Food Sci. Emerg. Technol.* **2020**, *60*, 102288. [CrossRef]
11. Pakhomov, A.G.; Pakhomova, O.N. The interplay of excitation and electroporation in nanosecond pulse stimulation. *Bioelectrochemistry* **2020**, *136*, 107598. [CrossRef]
12. Vižintin, A.; Marković, S.; Ščančar, J.; Miklavčič, D. Electroporation with nanosecond pulses and bleomycin or cisplatin results in efficient cell kill and low metal release from electrodes. *Bioelectrochemistry* **2021**, *140*, 107798. [CrossRef] [PubMed]
13. Breton, M.; Mir, L.M. Microsecond and nanosecond electric pulses in cancer treatments. *Bioelectromagnetics* **2012**, *33*, 106–123. [CrossRef] [PubMed]
14. Guionet, A.; Joubert-Durigneux, V.; Packan, D.; Cheype, C.; Garnier, J.P.; David, F.; Zaepffel, C.; Leroux, R.M.; Teissié, J.; Blanckaert, V. Effect of nanosecond pulsed electric field on Escherichia coli in water: Inactivation and impact on protein changes. *J. Appl. Microbiol.* **2014**, *117*, 721–728. [CrossRef]

15. Vernier, P.T.; Sun, Y.; Marcu, L.; Salemi, S.; Craft, C.M.; Gundersen, M.A. Calcium bursts induced by nanosecond electric pulses. *Biochem. Biophys. Res. Commun.* **2003**, *310*, 286–295. [CrossRef] [PubMed]
16. Deng, J.; Schoenbach, K.H.; Stephen Buescher, E.; Hair, P.S.; Fox, P.M.; Beebe, S.J. The Effects of Intense Submicrosecond Electrical Pulses on Cells. *Biophys. J.* **2003**, *84*, 2709–2714. [CrossRef]
17. Beebe, S.J.; Fox, P.M.; Rec, L.J.; Somers, K.; Stark, R.H.; Schoenbach, K.H. Nanosecond pulsed electric field (nsPEF) effects on cells and tissues: Apoptosis induction and tumor growth inhibition. In Proceedings of the PPPS 2001—Pulsed Power Plasma Science, Las Vegas, NV, USA, 17–22 June 2001.
18. Ringel-Scaia, V.M.; Beitel-White, N.; Lorenzo, M.F.; Brock, R.M.; Huie, K.E.; Coutermarsh-Ott, S.; Eden, K.; McDaniel, D.K.; Verbridge, S.S.; Rossmeisl, J.H.; et al. High-frequency irreversible electroporation is an effective tumor ablation strategy that induces immunologic cell death and promotes systemic anti-tumor immunity. *EBioMedicine* **2019**, *44*, 112–125. [CrossRef]
19. Dermol-Černe, J.; Miklavčič, D.; Reberšek, M.; Mekuč, P.; Bardet, S.M.; Burke, R.; Arnaud-Cormos, D.; Leveque, P.; O'Connor, R. Plasma membrane depolarization and permeabilization due to electric pulses in cell lines of different excitability. *Bioelectrochemistry* **2018**, *122*, 103–114. [CrossRef]
20. Sano, M.B.; Fan, R.E.; Cheng, K.; Saenz, Y.; Sonn, G.A.; Hwang, G.L.; Xing, L. Reduction of Muscle Contractions during Irreversible Electroporation Therapy Using High-Frequency Bursts of Alternating Polarity Pulses: A Laboratory Investigation in an Ex Vivo Swine Model. *J. Vasc. Interv. Radiol.* **2018**, *29*, 893–898. [CrossRef]
21. Redondo, L.M.; Zahyka, M.; Kandratsyeu, A. Solid-State Generation of High-Frequency Burst of Bipolar Pulses for Medical Applications. *IEEE Trans. Plasma Sci.* **2019**, *47*, 4091–4095. [CrossRef]
22. Pirc, E.; Miklavčič, D.; Uršič, K.; Serša, G.; Reberšek, M. High-frequency and high-voltage asymmetric bipolar pulse generator for electroporation based technologies and therapies. *Electronics* **2021**, *10*, 1203. [CrossRef]
23. Ryan, H.A.; Hirakawa, S.; Yang, E.; Zhou, C.; Xiao, S. High-Voltage, Multiphasic, Nanosecond Pulses to Modulate Cellular Responses. *IEEE Trans. Biomed. Circuits Syst.* **2018**, *12*, 338–350. [CrossRef] [PubMed]
24. Kandratsyeu, A.; Sabaleuski, U.; Redondo, L.; Pakhomov, A.G. Four Channel 6.5 kV, 65 A, 100 ns–100 µs Generator with Advanced Control of Pulse and Burst Protocols for Biomedical and Biotechnological Applications. *Appl. Sci.* **2021**, *11*, 1782. [CrossRef]
25. Butkus, P.; Murauskas, A.; Tolvaišiene, S.; Novickij, V. Concepts and capabilities of in-house built nanosecond pulsed electric field (nsPEF) generators for electroporation: State of art. *Appl. Sci.* **2020**, *12*, 4244. [CrossRef]
26. Huiskamp, T.; Van Oorschot, J.J. Fast Pulsed Power Generation with a Solid-State Impedance-Matched Marx Generator: Concept, Design, and First Implementation. *IEEE Trans. Plasma Sci.* **2019**, *47*, 4350–4360. [CrossRef]
27. López-Alonso, B.; Sarnago, H.; Lucía, O.; Briz, P.; Burdío, J.M. Real-time impedance monitoring during electroporation processes in vegetal tissue using a high-performance generator. *Sensors* **2020**, *11*, 3158. [CrossRef]
28. Novickij, V.; Stanevičienė, R.; Staigvila, G.; Gruškienė, R.; Sereikaitė, J.; Girkontaitė, I.; Novickij, J.; Servienė, E. Effects of pulsed electric fields and mild thermal treatment on antimicrobial efficacy of nisin-loaded pectin nanoparticles for food preservation. *LWT* **2020**, *120*, 108915. [CrossRef]
29. Novickij, V.; Ruzgys, P.; Grainys, A.; Šatkauskas, S. High frequency electroporation efficiency is under control of membrane capacitive charging and voltage potential relaxation. *Bioelectrochemistry* **2018**, *119*, 92–97. [CrossRef]
30. Pakhomov, A.G.; Grigoryev, S.; Semenov, I.; Casciola, M.; Jiang, C.; Xiao, S. The second phase of bipolar, nanosecond-range electric pulses determines the electroporation efficiency. *Bioelectrochemistry* **2018**, *122*, 123–133. [CrossRef]
31. Novickij, V.; Baleviciute, A.; Malysko, V.; Zelvys, A.; Radzeviciute, E.; Kos, B.; Zinkeviciene, A.; Miklavcic, D.; Novickij, J.; Girkontaite, I. Effects of Time Delay Between Unipolar Pulses in High Frequency Nano-Electrochemotherapy. *IEEE Trans. Biomed. Eng.* **2021**. [CrossRef]
32. Sundararajan, R. Nanosecond electroporation: Another look. *Mol. Biotechnol.* **2009**, *41*, 69–82. [CrossRef]
33. Pakhomov, A.G.; Gianulis, E.; Vernier, P.T.; Semenov, I.; Xiao, S.; Pakhomova, O.N. Multiple nanosecond electric pulses increase the number but not the size of long-lived nanopores in the cell membrane. *Biochim. Biophys. Acta—Biomembr.* **2015**, *1848*, 958–966. [CrossRef] [PubMed]
34. Schoenbach, K.H.; Hargrave, B.Y.; Joshi, R.P.; Kolb, J.F.; Nuccitelli, R. Bioelectric effects of intense ultrashort pulses. *Crit. Rev. Biomed. Eng.* **2010**, *38*, 255–304. [CrossRef] [PubMed]
35. Zhao, Y.; Bhonsle, S.; Dong, S.; Lv, Y.; Liu, H.; Safaai-Jazi, A.; Davalos, R.V.; Yao, C. Characterization of conductivity changes during high-frequency irreversible electroporation for treatment planning. *IEEE Trans. Biomed. Eng.* **2018**, *65*, 1810–1819. [CrossRef] [PubMed]
36. Aycock, K.N.; Zhao, Y.; Lorenzo, M.F.; Davalos, R.V. A theoretical argument for extended interpulse delays in therapeutic high-frequency irreversible electroporation treatments. *IEEE Trans. Biomed. Eng.* **2021**, *68*, 1999–2010. [CrossRef] [PubMed]
37. Pakhomov, A.G.; Xiao, S.; Novickij, V.; Casciola, M.; Semenov, I.; Mangalanathan, U.; Kim, V.; Zemlin, C.; Sozer, E.; Muratori, C.; et al. Excitation and electroporation by MHz bursts of nanosecond stimuli. *Biochem. Biophys. Res. Commun.* **2019**, *518*, 759–764. [CrossRef]
38. Semenov, I.; Casciola, M.; Ibey, B.L.; Xiao, S.; Pakhomov, A.G. Electropermeabilization of cells by closely spaced paired nanosecond-range pulses. *Bioelectrochemistry* **2018**, *121*, 135–141. [CrossRef]